

EOSAM 2023

Guest editors: Patricia Segonds, Guy Millot and Bertrand Kibler

RESEARCH ARTICLE

OPEN ACCESS

Parallel illumination for depletion microscopy through acousto-optic spatial light modulation

Fabian Klingmann^{1,2}, Nick Toledo-García¹, Estela Martín-Badosa^{1,3}, Mario Montes-Usategui^{1,3}, and Jordi Tiana-Alsina^{1,3,*} 

¹ Department de Física Aplicada, Facultat de Física, Universitat de Barcelona, Martí i Franquès 1, 08028 Barcelona, Spain

² Fraunhofer-Institut für Photonische Mikrosysteme (IPMS), Maria-Reiche-Str. 2, 01109 Dresden, Germany

³ Institut de Nanociència i Nanotecnologia (IN2UB), 08028 Barcelona, Spain

Received 31 January 2024 / Accepted 27 May 2024

Abstract. State-of-the-art super-resolution microscopy techniques, including Stimulated Emission Depletion (STED), Reversible Saturable Optical Fluorescence Transitions (RESOLFT), and Switching Laser Mode (SLAM) microscopies, implement Laguerre-Gaussian beams, also known as vortex or doughnut beams to capture fluorescence information within a sub-wavelength area of the observed sample, effectively surpassing the diffraction limit and significantly improving the quality of the image. However, these techniques typically operate at point by point basis, involving time-consuming scanning of the sample to construct a complete, meaningful image. Therefore, for real-time live cell imaging purposes, the parallelization of illumination is crucial. In this study, we demonstrate the parallel generation of arbitrary arrays of Gaussian and Laguerre-Gaussian laser foci suitable for super-resolution microscopy. We achieve rapid scanning through the sample using acousto-optic spatial light modulation, a technique we have previously pioneered across various fields. By employing parallelized illumination with both Gaussian and doughnut beams, we aim to capture super-resolution images.

Keywords: Parallel illumination, Acousto-optical devices, Super-resolution microscopy, Subtraction microscopy.

1 Introduction

Resolution is one of the most significant constraints in fluorescence microscopy, even for the edge-cutting technology confocal microscopes that are the most prevalent for visualization in many applications in the Life Sciences. It is no wonder, then, that the emergence of optical super-resolution, around the turn of the century [1, 2], has profoundly transformed the modern microscopy landscape. The emerging super-resolution techniques, Stimulated Emission Depletion (STED) and its variants (Ground State Depletion, GSD [3], Continuous Wave STED, CW-STED [4], Reversible Saturable Optical Fluorescence Transitions, RESOLFT [5, 6], and Minimum Emission Fluxes, MINFLUX [7]) are noteworthy for their exceptional resolution capabilities (reaching down to 1–2 nm for MINFLUX). Depletion microscopies like STED are based on the confinement of the fluorescent emission within a sub-wavelength region through the coordinated action of two lasers. The first laser beam presents a typical TEM₀₀ Gaussian intensity profile, and it is used to excite (or activate, in RESOLFT) the fluorophores within the sample. A second

laser beam, characterized by a “doughnut” intensity profile (i.e., a Laguerre-Gaussian beam), suppresses the spontaneous fluorescence (or deactivates the fluorophores) around the central singularity, leaving the molecules near the dark core unaffected. Consequently, the resulting fluorescent emission comes from a reduced, sub-diffractive area of the sample. The subsequent image is constructed by scanning the sample. The collection of emitted photons yields an effective point spread function (PSF) that achieves super-resolution within the range of 30–70 nm [1, 2]. While STED uses standard fluorophores, RESOLFT uses photoswitchable molecules, which drastically reduce the laser power needed for the depletion beam, thus inducing less photo-damage, making prolonged observation of living cells more feasible [5]. Nevertheless, one of the several drawbacks associated with STED and its derivatives is the relatively slow operation due to the sequential composition of images.

2 Acousto-optic deflectors (AODs) for parallel illumination

Despite the success of the implementation of highly parallel depletion microscopy setups, typically RESOLFT due to its

* Corresponding author: jordi.tiana@ub.edu

cell friendly properties, which significantly speed up the scanning process, as described in the literature [6, 8], these methods depend on the periodic minima of a standing wave illumination to confine fluorescence at multiple spots simultaneously. In this contribution, we present an alternative approach: the generation of extensive arrays of switchable Gaussian and Laguerre-Gaussian laser spots using acousto-optic holography. Acousto-optic deflectors (AODs) are TeO₂ crystal based beam-steering devices, wherein the refractive index is modulated by an acoustic wave generated with an oscillating piezoelectric transducer driven by an electrical signal. Recent studies have demonstrated the versatility of AODs as general-purpose spatial light modulators. This is achieved by computing driving signals using digital holography techniques and feeding the transducer with these signals via a programmable radiofrequency generator [9–11]. Within the crystal, a specific refractive index variation emerges, enabling spatial control over a laser beam as it traverses the device. The details of how we compute such holographic driving signals have been reported elsewhere [9–11]; however, throughout the next sections we show that properly designed acousto-optic holograms can be used as the basis for parallelizing the paired excitation/de-excitation beams essential in STED-like super-resolution microscopy. Additionally, acousto-optic holography offers a convenient method for rapidly scanning the sample using these illumination arrays, thereby presenting a promising technology for the development of future live-cell, optical super-resolution microscopes capable of operating at video rates. Although there are previous studies of the behavior of Laguerre-Gaussian beams after deflection by AODs, which show that their shape remains largely unaffected, these studies do not specifically consider their suitability for super-resolution microscopy [12, 13].

3 Experimental setup

In this work we aim to produce, assess, and validate the optical quality of TEM₀₁ Laguerre-Gaussian beams, also known as optical vortices or doughnut beams, after going through a pair of active acousto-optic cells with a view to parallelize STED-like super-resolution microscopy. To accomplish this goal, we will utilize the experimental setup depicted in Figure 1, which employs a two-path scheme illuminated with a TEM₀₀ Gaussian beam. The illumination laser source is a $\lambda = 488$ nm laser (Integrated Optics, MatchBox 0488L-15A-NI-PT-NF). The setup offers flexibility in controlling the active light path by adjusting the input polarization using a half-wave plate placed on a rotation mount that allows for precise tuning at the entrance port of the polarizing beam splitter. In one of the paths, the TEM₀₁ Laguerre-Gaussian mode is generated when a Gaussian beam passes through a vortex phase plate. A vortex phase plate or spiral phase plate consists of a dielectric coating plate whose thickness increases in a given number of steps, proportionally to the azimuth angle around a point in the center [14]. The Vortex-Photonics phase plate (V-488-10-1) possesses 64 steps, and is tuned to our working wavelength ($\lambda = 488$ nm) with a topological charge $m = 1$.

On the other path, the input TEM₀₀ Gaussian mode is freely propagated. A second half-wave retarder is placed after a polarizing beam-splitter that again merges the two optical trains. By always moving both $\lambda/2$ -plates by the same angle, the polarization at the AOD will not change. Two mirrors are then used to align the beam with the camera port of the microscope. Since metallic mirrors were used, it was necessary to place a linear polarizer after them, to filter out undesired polarization components. The image acquisition time of this setup is currently limited by the rotation time of the $\lambda/2$ -plates, which takes around 100 μ s to complete the 45° travel needed to change between input and output polarization states. Finally, either the Gaussian or the doughnut beam enters into our microscope (Nikon Eclipse TE2000) equipped with a high numerical aperture objective (Nikon CFI PlanApo λ D, oil-immersion, 100 \times , NA = 1.45). As previously mentioned, in order to create a 2D spot array for illuminating the sample, two AODs are employed (Fig. 1, upper right inset). The scanning of the sample along the horizontal and vertical directions is achieved by shifting the illumination pattern through a linear phase ramp introduced into the hologram (since there is a Fourier transform relationship between the AODs and the objective focal plane). To image a sample with a field of view spanning $66 \times 66 \mu$ m, we employed an illumination matrix consisting of 20×20 points, featuring Gaussian or doughnut beams, each spaced 3.3μ m apart. This illumination matrix scanned the sample in 20×20 steps. For each scanning step the sample was exposed for 10 ms for a resulting frame rate around 0.25 Hz (corresponding to the images shown in the manuscript). With the reported prototype, we could eventually achieve a frame rate of one image per second, by reducing the exposure time and compensating for with an increased illumination power.

Based on this scheme, we have designed and implemented, at a proof of concept level, a microscope capable of parallelizing the illumination. In what follows, we will provide results that demonstrate the capacity of this instrument for super-resolution microscopy, for which we will employ an algorithm based on the subtraction between the images obtained with Gaussian and doughnut illuminations.

4 Weighted subtraction microscopy approach

As described in [15, 16], subtraction microscopy is a technique that involves illumination with both a Gaussian and a doughnut beam, which leads to a super-resolution comparable to that provided by structured illumination microscopy. Subtraction microscopy is a cost-effective implementation of STED microscopy, a type of laser scanning microscopy where two fluorescent images are taken, one when illuminated by a standard Gaussian and one with a doughnut profile, as the excitation beams. The doughnut-illuminated image is then subtracted from the Gaussian-illuminated image with a weighting factor α :

$$I_{im}(x, y) = I_g(x, y) - \alpha \cdot I_d(x, y) \quad (1)$$

The choice of the α factor has a large influence on the image quality and resolution. A value that is too small will not

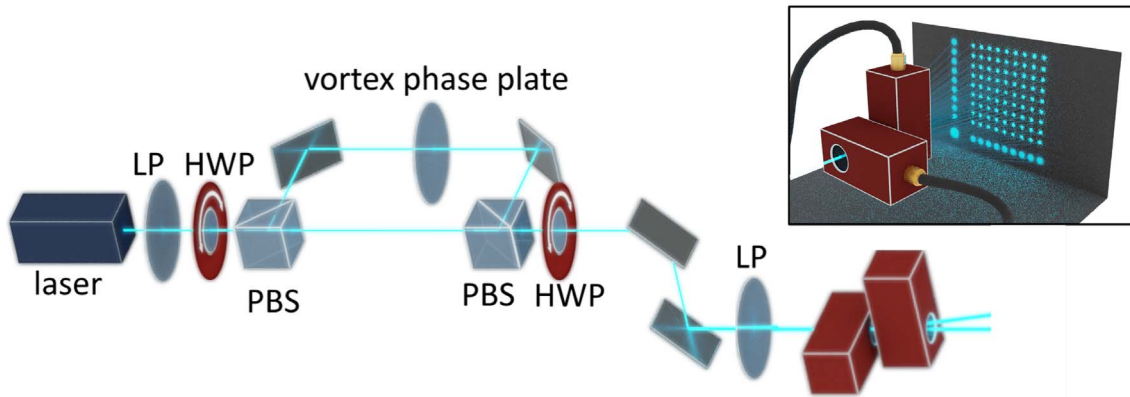


Figure 1. Experimental setup for the characterization of the doughnut beam. (LP) linear polarizers, (HWP) half-wave plates mounted in rotation mounts, (PBS) polarizing beam splitters. The upper right inset shows the two AOD configuration used to generate the 2D illumination spot array.

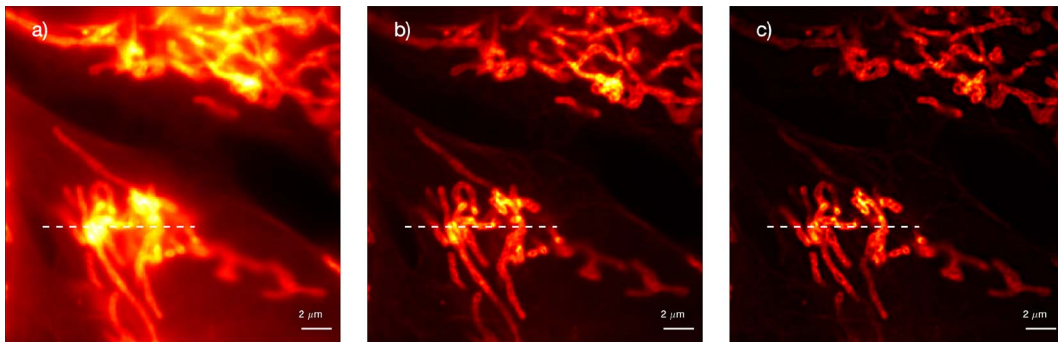


Figure 2. Images of mitochondria in huFIB cells synthesized with (a) epifluorescence, (b) virtual pinhole with Gaussian illumination and (c) virtual pinhole with subtraction algorithms. For the subtraction algorithm, a constant coefficient of $\alpha = 0.58$ was chosen.

lead to an increase in resolution, whereas too large a value will produce artifacts in the final image. We have found that a factor $\alpha = 0.58$ leads to maximum resolution without visible artifacts in our case.

5 Results

We show in [Figure 2](#) the reconstructed images of mitochondria in human fibroblasts labelled with Alexa Fluor 488 (Cells 4c, GATTAquant). In [Figure 2\(a\)](#) epifluorescence images are synthesized by assigning to each pixel the averaged value of that pixel in all images gathered under Gaussian illumination. As expected, under this reconstruction algorithm, the background from out-of-focus light is quite prominent.

In [Figure 2\(b\)](#) we used a virtual pinhole reconstruction algorithm, imitating the physical pinhole of confocal microscopy, where each point of the captured image is multiplied by a Gaussian mask with a size of the effective point spread function (PSF), in our case this was chosen to be 195 nm). This method allows for the capture of optical sections of samples with improved resolution and

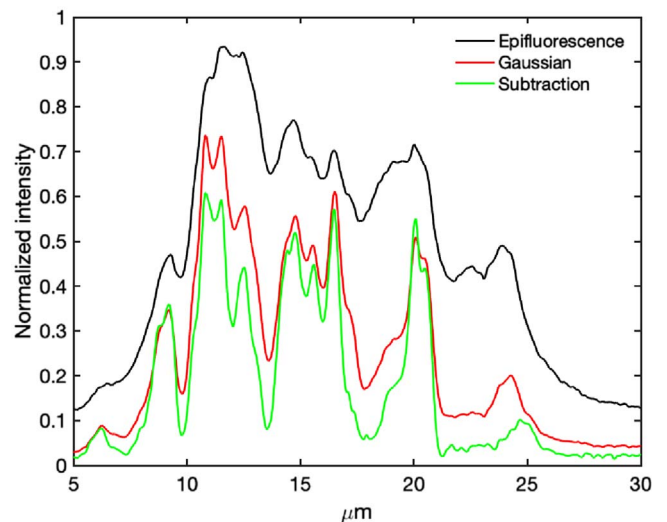


Figure 3. Intensity profiles extracted from dashed white lines in [Figure 2](#) corresponding to epifluorescence (black line), virtual pinhole with Gaussian illumination (red line), and virtual pinhole with subtraction (green line) reconstructed images.

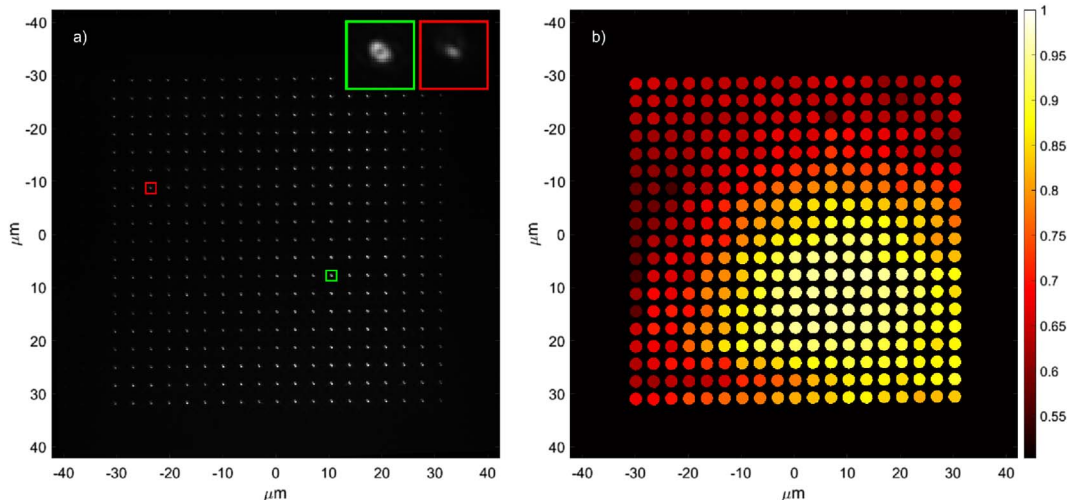


Figure 4. (a) Image of the doughnut illumination pattern using a mirror sample and (b) R^2 map to quantify the quality of doughnuts. The red and green squares represent the doughnut spots with the lowest and highest R^2 values within the array, respectively.

reduced background noise. Under this algorithm, a clear improvement in terms of out-of-focus light is observed, although the images still do not show super-resolution information.

Finally, in Figure 2(c) the reconstructed image using the subtraction algorithm in combination with the two illuminations (Gaussian/Laguerre-Gaussian) and virtual pinholing is presented. A clear improvement in both out-of-focus light and resolution can be appreciated.

In order to qualitatively assess the enhancement in resolution achieved by the three implemented algorithms in Figure 3, we present a horizontal cross-section (indicated by the dashed white line in Fig. 2). This figure demonstrates a noticeable improvement in both background intensity and resolution. Particularly with the subtraction algorithm, significantly finer intensity peaks are evident, characterized by a reduced full width at half maximum of the mitochondria membrane sections.

Furthermore, in order to quantitatively evaluate the resolution of these images, the ImageJ plugin presented in [17] is used. The resolution obtained is 230 nm, 200 nm and 136 nm for epifluorescence, Gaussian pinholing and subtraction with pinholing methods, respectively. With respect to the Abbe diffraction limit, $\Delta x = \frac{\lambda}{2NA} = 190$ nm for a wavelength of 488 nm and an effective numerical aperture of 1.33, we have achieved a $\sqrt{2}$ improvement factor.

Finally, in order to illustrate the quality of the doughnuts across the entire field of view, we examine their characteristics. As discussed in [18], doughnut beams are highly sensitive to off-axis deformations and very particularly to astigmatic aberrations. In Figure 4, it is evident that the quality of the doughnuts, characterized by the R^2 factor obtained from the 2D fitting of the doughnut modes, deteriorates as we move radially away from the optical axis. It is worth noting that in our setup, the optical axis is slightly shifted to the bottom right corner of the image.

6 Conclusions

In this work we have presented a proof of concept microscope, based on AODs technology to parallelise both Gaussian and doughnut illumination, capable of obtaining super-resolution images with a subtraction-based algorithm. Even though we already obtained super-resolved images, we anticipate a better resolution in the future when addressing the correction of astigmatic aberrations in our setup.

Currently, the main time limitation comes from the rotational mounts that control the input and output polarization states (that switch from Gaussian to doughnut illumination), but in future implementations we expect to reduce it by using two lasers and triggering signals. Then the imaging time will mainly depend on the exposure time and the number of steps in the scanning process, but since the scanning is parallelized, a significant reduction compared to conventional laser scanning microscopes will be easily achieved.

Acknowledgments

We thank Raül Bola for his previous development of a parallel confocal microscope, which significantly facilitated our own research and development efforts. Furthermore, we are grateful for his valuable insights and informal scientific discussions, which have greatly contributed to the advancement of our work.

Funding

This work was supported by grant PREP2022-000292, funded by MICIU/AEI/10.13039/501100011033 and ESF+, by grant PID2022-136796OB-I00, funded by MCIN/AEI/10.13039/501100011033/FEDER, UE, by Ministerio de Ciencia e Innovación (PDC2022-133351-I00 and PID2022-136796OB-I00), and Fundació Bosch i Gimpera (F2I-PdC-2023-008-600427).

Author contribution statement

Fabian Klingmann: Investigation (equal); Software (equal); Validation (equal); Formal analysis (equal); Visualization (equal); Writing – original draft (equal); Writing – review & editing (equal). **Nick Toledo-García:** Software (equal); Validation (equal); Formal analysis (equal); Writing – review & editing (equal). **Estela Martín-Badosa:** Conceptualization (equal); Visualization (equal); Writing – original draft (equal); Writing – review & editing (equal); Funding acquisition (equal). **Mario Montes-Usategui:** Conceptualization (equal); Visualization (equal); Writing – original draft (equal); Writing – review & editing (equal); Funding acquisition (equal). **Jordi Tiana-Alsina:** Conceptualization (equal); Investigation (equal); Visualization (equal); Writing – original draft (equal); Writing – review & editing (equal); Funding acquisition (equal).

References

- 1 Lakadamyali M. (2014) *ChemPhysChem* **15**, 630.
- 2 Sahl S.J., Hell S.W. (2019) *High-resolution 3D light microscopy with STED and RESOLFT*, Springer International Publishing, Cham.
- 3 Hell S.W., Kroug M. (1995) *Appl. Phys. B* **60**, 495.
- 4 Willig K.I., Harke B., Medda R., Hell S.W. (2007) *Nat. Methods* **4**, 915.
- 5 Hofmann M., Eggeling C., Jakobs S., Hell S.W. (2005) *Proc. Natl. Acad. Sci.* **102**, 17565.
- 6 Chmyrov A., Keller J., Grotjohann T., Ratz M., d'Este E., Jakobs S., Eggeling C., Hell S.W. (2013) *Nat. Methods* **10**, 737.
- 7 Balzarotti F., Eilers Y., Gwosch K.C., Gynnå A.H., Westphal V., Stefani F.D., Elf J., Hell S.W. (2017) *Science* **355**, 606.
- 8 Masullo L.A., Bodén A., Pennacchietti F., Coceano G., Ratz M., Testa I. (2018) *Nat. Commun.* **9**, 3281.
- 9 Treptow D., Bola R., Martín-Badosa E., Montes-Usategui M. (2021) *Sci. Rep.* **11**, 21261.
- 10 Bola R., Treptow D., Marzoa A., Montes-Usategui M., Martín-Badosa E. (2020) *Opt. Lett.* **45**, 2938.
- 11 Montes-Usategui M., Bola R., Martín-Badosa E., Treptow D. (2019) Programmable multiple-point illuminator, confocal filter, confocal microscope and method to operate said confocal microscope, PCT/EP2019/067517.
- 12 Mur J., Kavčič B., Poberaj I. (2013) *Appl. Opt.* **52**, 6506.
- 13 Martynyuk-Lototska I., Vasylyuk Y., Dudok T., Skab I., Vlokh R. (2018) *Optik* **155**, 179.
- 14 Beijersbergen M.W., Coerwinkel R.P.C., Kristensen M., Woerdman J.P. (1994) *Opt. Commun.* **112**, 321.
- 15 Korobchevskaya K., Peres C., Li Z., Antipov A., Sheppard C.J.R., Diaspro A., Bianchini P. (2016) *Sci. Rep.* **6**, 25816.
- 16 Kuang C., Li S., Liu W., Hao X., Gu Z., Wang Y., Ge J., Li H., Liu X. (2013) *Sci. Rep.* **3**, 1441.
- 17 Descloux A., Größmayer K.S., Radenovic A. (2019) *Nat. Methods* **16**, 918.
- 18 Ohland J.B., Eisenbarth U., Roth M., Bagnoud V. (2019) *Appl. Phys. B* **125**, 202.